ACS APPLIED MATERIALS & INTERFACES

Research Article

www.acsami.org

Controllable Nitrogen Doping of High-Surface-Area Microporous Carbons Synthesized from an Organic–Inorganic Sol–Gel Approach for Li–S Cathodes

Huichao Chen,[†] Yanju Wei,[†] Jitong Wang,[†] Wenming Qiao,[†,‡] Licheng Ling,[†,‡] and Donghui Long*[,†,‡]

[†]State Key Laboratory of Chemical Engineering, East China University of Science and Technology, Shanghai 200237, China

[‡]Key Laboratory of Specially Functional Polymeric Materials and Related Technology, East China University of Science and Technology, Shanghai 200237, China

Supporting Information

ABSTRACT: High-surface-area microporous carbons with controllable nitrogen doping were prepared via a novel organic–inorganic sol–gel approach, using phenolic resol and hexamethoxymethyl melamine (HMMM) as carbon precursors, and partially hydrolyzed tetraethoxysilane as silica template. The pore structures of microporous carbons were completely replicated from a thin silica framework and could be tailored greatly by changing the organic/inorganic ratio. The nitrogen atoms doped into the carbon framework were issued from high-nitrogen-content HMMM precursors, and the nitrogen content could be adjusted in a wide range by changing the phenolic resol/HMMM ratio. Moreover, the porous structure and nitrogen content could be simultaneously controlled, allowing the preparation of a series of microporous carbons with almost the same microstructures (BET surface areas of ca.1900 $m^2 \cdot g^{-1}$and pore volumes of ca. 1.2 $cm^3 \cdot g^{-1}$, and the same pore size distributions) but with different nitrogen contents (0–12 wt %). These results provided a general method to synthesize nitrogen-doped microporous carbons and allowed these materials to serve as a model system to illustrate the role of nitrogen content on the performance of the carbons. When used as the supports for sulfur cathodes, only an appropriate nitrogen content of ca. 6.3 wt % was found to effectively improve sulfur utilization and cycle life of the sulfur cathodes. The resulting sulfur cathodes could deliver an outstanding reversible discharge capacity of 1054 mAh·g^{-1} at 0.5 C after 100 cycles.

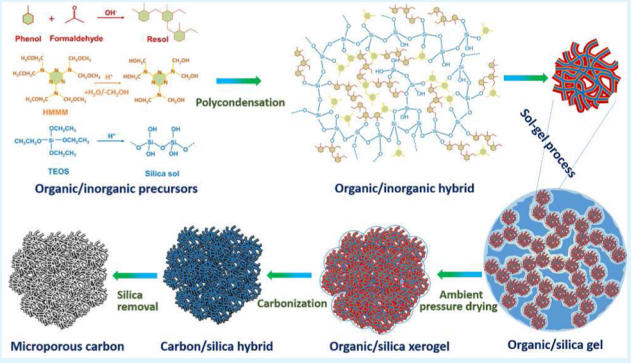

KEYWORDS: *microporous carbon, nitrogen doping, microstructure control, Li–S cathode, electrochemical performance*

1. INTRODUCTION

Microporous carbon is considered to have pore size mainly less than 2 nm in width and surface areas greater than 1000 $m^2 \cdot g^{-1}$.[1] Owing to its high degree of microporosity, good conductivity, and excellent thermal and chemical stability, it has been widely employed for various applications related to energy, environment, adsorption, catalysis, etc.[2−4] For many years, microporous carbons, especially activated carbons have been produced by carbonization and consequent physical/chemical activation of carbonaceous precursors.[5,6] These methods can create a developed porosity but a broad range of pore sizes, from visible cracks to gaps and slit-type voids of molecular dimensions.[7] For some specific uses, it is not always desirable to have a broad range of pore sizes. For example, storage of gases frequently requires small pores only, and thus, a uniform microporous carbon would be highly desirable.[8,9] Zeolite templating has been the most successful method so far in controlling the micropore size for the carbons.[10−12] However, its limitations involve the formation of nonporous carbon on the exterior of the template, high cost, and tedious and time-consuming infiltration steps.[13] Thus, it still remains a great challenge to fabricate well-defined microporous carbons with a facile and few-step approach.

The adsorption capacity and interfacial properties of microporous carbon depend on the pore structure, but also on the chemical nature of its surface, especially these oxygen- and nitrogen-containing surface functional groups. The oxygen functionalities, including the alcohol, the ether, the aldehyde, the ketone, and the carboxylic are always present on the carbon surface, generally contributing to an acidic character to the carbons.[14] The nitrogen functionalities are often directly doped into the carbon framework, basically in the formation of pyridinic N, pyrrolic N, graphitic N, and pyridine N-oxide.[14] These nitrogen groups could provide hydrophilic ability and Lewis basic properties, enhancing the interactions of adsorbed molecules with the carbon surface.[3,5,15] Moreover, nitrogen

Received: June 9, 2015
Accepted: September 12, 2015
Published: September 12, 2015

DOI: 10.1021/acsami.5b05107
ACS Appl. Mater. Interfaces 2015, 7, 21188–21197

functionalities could modify the electronic and crystalline structures of the carbons, thus changing their chemical stability, electronic conductivity, and electron-donor properties.[16−18] As a result, nitrogen-doped microporous carbons show improved performance in their wide applications, such as CO_2 adsorption,[19] anodes for Li-ion batteries,[20] and electrochemical supercapacitor electrodes.[21,22]

In the past decade, great efforts have been made to dope nitrogen atoms into microporous carbon via direct pyrolysis or co-carbonization of nitrogen-rich precursors. For example, Kyotani et al.[23] employed a zeolite Y templating method to prepare nitrogen-doped microporous carbons. They doped 6 wt % nitrogen atoms into the carbons by chemical vapor deposition of acetonitrile, which significantly improved the affinity and adsorption capacity toward H_2O molecules. Mokaya et al.[24] employed a similar method to generate microporous carbons with 4.7−7.7 wt % nitrogen doping, and they demonstrated that nitrogen doping could improve the hydrogen storage capacity. Xia et al.[25] prepared nitrogen-doped microporous carbons using acetonitrile as precursor, and they concluded that the sample with a moderate nitrogen content of 5.2 wt % exhibited the best CO_2 adsorption performance. However, the effect of the nitrogen doping level on the performance of the microporous carbons is rarely studied, possibly due to the difficulty in the synthesis of the carbons with controllable nitrogen doping. Meanwhile, the porosity of the carbons is always varied with the nitrogen doping, making it difficult to obtain a reliable conclusion on the nitrogen doping effect.

The Li−S battery is expected to be the next-generation energy storage system with many advantages like high capacity, high specific energy density, and low cost. However, several problems such as poor cycle life, high self-discharge, and low utilization of sulfur restrict their applications.[26] In response to these problems, coupling sulfur with conductive porous carbons has been researched extensively.[27−29] In spite of their various frameworks, pore size distribution is an important factor that determines the electrochemical performance of the batteries. The micropore is considered to encapsulate/immobilize the active material, which improves the electrochemical activity and suppresses the loss of active material.[30−32] The macropore can act as the pathway of electrolyte to ensure good electrolyte immersion. The mesopore usually serves as an essential supporter for strengthening the physical properties of the micropore or the macropore framework.[33,34] For cyclic stability of Li/sulfur batteries, the effect of micropore adsorption has been proved to lead to the best results,[35] while surface functionalization, especially nitrogen doping, can potentially improve this further. However, Li−S batteries using nitrogen-doped microporous carbons as cathodes have not been fully investigated, possibly due to the difficulty in simultaneously controlling the structure and nitrogen doping level of microporous carbons.

Here, in this work, we demonstrated a facile organic−inorganic sol−gel approach to obtain high-surface-area microporous carbons with well-defined microporosity and adjustable nitrogen doping. The synthesis method is the direct sol−gel polymerization of low-molecular-weight phenolic resol, high-nitrogen-content hexamethoxymethyl melamine (HMMM),[36] and partial-hydrolyzed TEOS, followed by the ambient drying, carbonization, and silica removal. The keys to this synthesis rely on not only the creation of uniform micropores replicating the low-degree-hydrolysis silica template but also a tunable nitrogen doping level (0−12 wt %) issued from the HMMM precursor. This approach, which could eliminate the tedious and time-consuming infiltration steps and provide control over both micropore structure and nitrogen-doped surface chemistry is, therefore, highly desirable. Moreover, the precisely controlled nitrogen doping level but with a similar pore size distribution may allow these materials to serve as excellent model systems for microporous carbons in general, to illustrate the role of nitrogen doping on the application performance of microporous carbons. To exemplify it, here we prepared a series of materials with different nitrogen contents and similar microporous structures to house sulfur for lithium−sulfur (Li−S) cathodes. The results give a solid proof that only an appropriate level of nitrogen doping could improve sulfur utilization and cycle life of the sulfur/carbon composites. The proof-of-concept study of the relationship between nitrogen doping level and electrochemical performance may provide some reference information for various microporous carbon material design and related applications.

2. EXPERIMENTAL SECTION

2.1. Material Preparation. HMMM (97% in *n*-propanol) was purchased from Ningbo Liuhua Polymer Co., LTD without further treatment. Phenolic resol dissolved in ethanol (50 wt %) was prepared from phenol and formaldehyde according to Zhao's previous reports.[37] Here, the molecular weight of resol was ca. 380 determined by GPC analysis (Figure S1, Supporting Information). Silica sols with a concentration of 13 wt % were prepared by hydrolysis of TEOS in the mixture of ethanol and HCl aqueous solution, giving a molar composition of 1.0 TEOS:0.007 HCl:3.5 H_2O:4.5 EtOH. The hydrolysis time was carefully controlled to be 30 min before mixing with the HMMM and phenolic resol.

The mixture alcogels were obtained by a sol−gel process of HMMM, phenolic resol, and silica sol at 80 °C. In a typical process, 15 g of phenolic resol solution (50 wt % in ethanol) was mixed with 7.5 g of HMMM and stirred for 10 min to form a homogeneous solution; after that, 70 g of silica solution (13 wt %) was added dropwise and the mixture was stirred for 30 min to form a pale yellow solution. The as-prepared solution was sealed and aged at 80 °C in a water bath to obtain transparent alcogel. The obtained gels were then dried at 80 °C at an ambient pressure condition, followed by the carbonization at 800 °C for 3 h with a heating rate of 3 °C min^{-1} in a nitrogen flow. The nitrogen-doped microporous carbons (NMCs) were obtained by dissolution of the silica nanoparticles in 2 M NaOH solution at 80 °C for 12 h, isolated by filtration, washed with distilled water until the pH did not change, and dried at 100 °C.

To precisely adjust the nitrogen doping level while keeping the porosity similar, herein the mass ratio of carbon/silica was fixed while the mass ratio of HMMM:phenolic resol:silica in the precursors was changed as 0/15/15, 5/10/11, 7.5/7.5/9, and 10/5/7, respectively. The obtained samples are denoted as NMC-*x*, where *x* represents for the mass ratio of HMMM to phenolic resol.

In addition, the microporous structure of the carbons can also adjusted by changing mass ratio of carbon/silica. To exemplify it, a series of nitrogen-free samples were prepared at the mass ratio of silica to phenolic resol of 0.8, 1, 1.2, and 1.5, respectively. These samples are denoted as NMC-0 (*y*:1), where *y* represents the mass ratio of silica to phenolic resol.

2.2. Preparation of NMC/S Composites. The NMC/S composites were prepared using a conventional melt-diffusion approach.[38] Typically, 0.2 g of sublimed sulfur and 0.3 g of NMCs were mixed homogeneously. The mixture was degassed in a vessel and then sealed under vacuum. A melt infiltration was carried out inside the vacuum-sealed vessel at 155 °C for 10 h. The temperature was then increased to 300 °C for another 2 h in order to vaporize superfluous sulfur on the outer surface of the NMCs, diffusing entirely

DOI: 10.1021/acsami.5b05107
ACS Appl. Mater. Interfaces 2015, 7, 21188−21197

Scheme 1. Schematic Illustration of the Preparation of Nitrogen-Doped Microporous Carbons

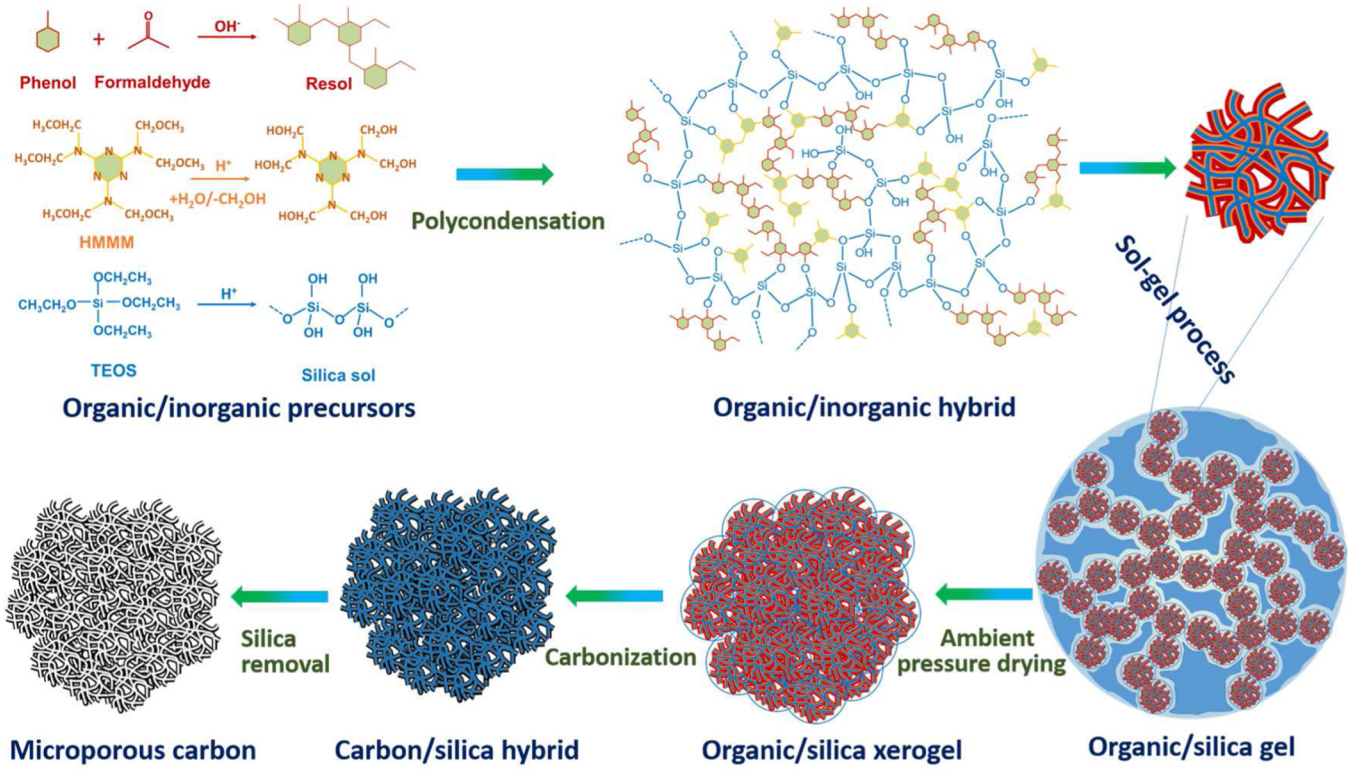

into the pores. The NMC/S composites were denoted as NMC/S-*x*, where *x* stands for the mass ratio of HMMM to phenolic resol.

2.3. Characterization. The average molecular weight (Mw) of the phenolic resol was determined by gel permeation chromatography (PL-GPC50, Polymer Laboratories). The phenolic resol was dissolved in tetrahydrofuran (THF). Polystyrene standards were used to generate the calibration curve. This test was conducted using THF as a carrier solvent at 40 °C with a flow rate of 1 mL·min^{-1}.

Elemental analysis (EA) was carried out with a varioMicro cube elemental analysis instrument using Elemental Vario EL III. The carbon (C), hydrogen (H), and nitrogen (N) contents of the carbons were determined directly using the thermal conductivity detector.

The thermogravimetric analysis (TA Instrument Q600 Analyzer) was carried out at a nitrogen or air flow rate of 100 mL min^{-1}. The samples were heated to the target temperature with a heating rate of 10 °C min^{-1}.

The surface composition of the NMCs was obtained by using X-ray photoelectron spectroscopy (Axis Ultra DLD). The operation voltage and current of the X-ray source were 15 kV and 10 mA, respectively. The working pressure was lower than 2×10^{-8} Torr. The C 1s, N 1s, and O 1s XPS spectra were measured at a 0.1 eV step size. All the element binding energies were referenced to the C 1s line situated at 284.6 eV. The N 1s XPS signals were fitted with mixed Lorentzian−Gaussian curves, and a Shirley function was used to subtract the background using an XPS peak processing software. The peak width was not fixed during the fit procedure.

The X-ray diffraction (XRD) patterns were recorded on a Rigaku D/max 2200 PC diffractometer with Cu Kα radiation (40 kV and 20 mA, λ = 1.5406 Å). Raman spectra were carried out on a Renishaw system 1000 with an argon-ion laser operating at 514 nm with a charge coupled device detector.

Transmission electron microscopy (TEM) images and field emission scanning electron microscopic (SEM) images were obtained by a JEOL-2010F electron microscope operating at 200 kV and a HitachiS-4800, respectively.

Nitrogen adsorption/desorption measurements for NMCs and NMC/S composites were carried out on a Quadrasorb SI analyzer at 77 K. Before the measurements, the NMCs were first degassed in vacuum at 453 K for at least 10 h, while the NMC/S composites were degassed under vacuum at 303 K for at least 12 h. The specific surface area was calculated based on the Brunauer−Emmett−Teller (BET) method while the total pore volume was obtained using a single point at a relative pressure of 0.985. The pore size distributions (PSDs) were derived from the adsorption branch by using the Quenched Solid Density Functional Theory (QS-DFT) model.

The electrical conductivity measurements were obtained at ambient temperature using the four-contact method. The NMCs were filled in a Teflon cylinder with an inner diameter of 16 mm, and two stainless-steel plungers were used to deliver 4 MPa pressure through a hydraulic press device. The voltage and current through stainless-steel plungers were recorded by using two Keithley 2000 digital multimeters. The electrical conductivity was calculated on the basis of the powder electrical resistivity. In a control experiment, the electronic conductivity of carbon black (Super P) is measured as 2.5 S/cm.

2.4. Electrochemical Measurement. The NMC/S composites were slurry-cast onto a carbon-rich aluminum current collector. Typically, 80 wt % NMC/S composites, 10 wt % carbon black (Super P Conductive Carbon Black), and 10 wt % binder (PVDF) were dissolved in *N*-methyl-2-pyrrolidone (NMP) and stirred for 3 h to form a homogeneous slurry. The slurries were then coated onto the carbon-rich aluminum current collectors and dried at 50 °C for at least 10 h. The active materials coated aluminum was then cut into a disk (12 mm in diameter) with a sulfur mass loading of 0.7 mg·cm^{-2}. Electrochemical measurements of these NMC/S composites were performed using coin cells with a sulfur composite cathode and lithium metal as the counter electrode, 1 M bis(trifluoromethane)sulfonamide lithium salt (LiTFSI) dissolved in a mixture of 1, 3-dioxoane (DOL) and dimethoxyethane (DME) (1:1 by volume), containing 0.25 M $LiNO_3$ as electrolyte, and a microporous membrane (Celgard 2400) as separator. The coin cells were assembled in a glovebox filled with argon. Cyclic voltammetry measurements (CV) were performed using an Arbin battery cycler (Arbin BT2000, USA). The galvanostatic charge−discharge tests were performed using a Land battery tester (LAND, CT2001C, China).The capacity values were calculated based on the sulfur mass. Electrochemical impedance spectroscopy (EIS) was characterized by using an electrochemical working station PCI4/

DOI: 10.1021/acsami.5b05107
ACS Appl. Mater. Interfaces 2015, 7, 21188−21197

300 (Gamry Instrument, Warminster, PA, USA). The sinusoidal excitation voltage was 5 mV, while the frequence range was from 100 kHz to 0.01 Hz. All of these electrochemical tests were carried out at ambient temperature.

3. RESULTS AND DISCUSSION

3.1. Characterization of NMCs. The total synthesis of NMCs is illustrated in Scheme 1. The synthesis starts with a sol−gel process of phenolic resol, HMMM, and partial-hydrolyzed TEOS. Transparent organic−inorganic hybrid gel (Figure S2, Supporting Information) can thus be formed via a phase separation induced by the co-condensation or hydrogen bonding interactions of these −OH functionalized oligomers. The hybrid gel is then directly dried at the ambient pressure conditions, leaving a dense and nonporous organic−inorganic hybrid solid due to the severe capillary pressures, followed by the carbonization and silica etching. NMCs are obtained in which the uniform micropores are completely replicated from the silica template while the nitrogen atoms doped are issued from the HMMM. The mild sol−gel process allows the formation of hybrid gels in any desired ratios of three components, leading to the highly controllable microporous structure as well as nitrogen doping level. It is noted that the gelation time remarkably decreases from 3 days to only a few hours if HMMM is added. Thus, HMMM serves not only as nitrogen source for the carbon but also as a cross-linked promoter for the sol−gel transition of the system.

The typical morphology of the obtained NMCs is observed by SEM and TEM, as shown in Figure 1. The SEM image

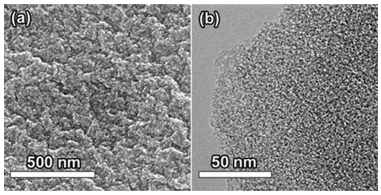

Figure 1. Typical SEM (a) and TEM (b) images of NMC-0.5.

reveals that the NMCs consist of dense nanoparticles inherited from the sol−gel network. It is hard to find any mesoporous or macroporous structure, further confirming the complete collapse of the gel network during the ambient pressure drying. TEM image shows clearly a disordered structure with randomly intersectant "white" and "black" stripes, indicating that the pore structure mainly consists of interconnected nanochannels that should directly resemble the silica template. The average diameter of nanochannels is estimated to be ca. 1−2 nm. There is no obvious difference between nitrogen-doped and nitrogen-free microporous carbons observed from TEM images (Figure S3, Supporting Information).

The pore structures are completely replicated from the silica; thus, the ratio of the carbon precursor to the silica precursor dramatically influences the surface area and pore volume of the resulting carbons. To illustrate this, a series of microporous carbons were prepared by changing the mass ratio of silica/phenolic resol from 0.8 to 1.5. The nitrogen adsorption−desorption isotherms and resulting pore size distributions of these samples are shown in Figure 2a,b, respectively. The isotherms are largely similar regardless of the adsorption amount. All the samples possess a very similar type I isotherm with significant adsorption below a relative pressure P/P_0 of 0.1, corresponding to a typical microporous structure. The pore size distributions determined using the QS-DFT model indicate that the carbons consist of two peaks located at 1.2 and 2 nm, being mostly in the range of micropores. According to the QS-DFT model, the micropores (<2 nm) contribute to 55−57% of the total BET surface area and 50−60% of the total pore volume. The almost same pore size distributions reveal that silica templating generates a set of carbon materials with a highly similar pore channel system. This result also indicates that the silica nanoparticles do not grow during the sol−gel process, possibly due to the formation of the organic−inorganic hybrid structure. The detailed porous parameters are summarized in Table 1. The BET surface area and total pore volume of these carbons are in the ranges of 1720−2260 $m^2 \cdot g^{-1}$ and 0.9−1.3 $cm^3 \cdot g^{-1}$, respectively, generally increasing with the increase of silica/phenolic resol mass ratio. However, once the silica/phenolic resol mass ratio increases to 1.5, the BET surface area and total pore volume of the sample decrease dramatically to 1500 $m^2 \cdot g^{-1}$ and 1.1 $cm^3 \cdot g^{-1}$, respectively. The excessive silica template may cause a very thin carbon framework, leading to the partial pore collapse during silica etching and drying process.

The nitrogen atoms doped are issued from the HMMM; thus, the nitrogen doping level could be easily adjusted by changing the amount of HMMM used. However, because of different carbonization yields of phenolic resol (∼50%) and HMMM (∼10%), the nitrogen doping level could always change together with the porosity if we only change the mass ratio of HMMM to phenolic resol. To precisely adjust the nitrogen doping level while keeping the porosity similar, here we fixed the carbon/silica mass ratio and changed the HMMM/phenolic resol mass ratio. Four ratios of HMMM/phenolic resol/silica (0/15/15, 5/10/11, 7.5/7.5/9, and 10/5/7, respectively) were employed in this work. The TG analysis could well confirm that the resulting carbon/silica hybrid composites have almost the same carbon/silica mass ratios (Figure S4, Supporting Information), thus guaranteeing the similar porosity for the obtained NMCs. As shown in Figure 2c,d, these NMCs have almost the same adsorption−desorption isotherms and pore size distributions. They exhibit very close BET surface areas of ca. 1900 $m^2 \cdot g^{-1}$, total pore volumes of ca. 1.2 $cm^3 \cdot g^{-1}$, and the same pore size distributions with an average pore diameter of 2.0 nm (Table 1). The similar structural characteristics will minimize the effect of porosity, prompting us to focus only on nitrogen doping on the properties of the resulting carbons.

TG analysis (Figure S5, Supporting Information) of these NMCs with different nitrogen contents indicates a residual ash of typically less than 1%, suggesting that these carbons are virtually silica-free. The CHN compositions of these NMCs were measured by elemental analysis, as listed in Table 2. The nitrogen content can be easily controlled in a wide range from 0 to 12.1 wt % by changing the amount of HMMM used. It is noteworthy that the nitrogen content in this work is as high as 12.1%, which is, to our knowledge, among the highest in the microporous carbons typically for these with the high surface area of up to 1000 $m^2 \cdot g^{-1}$.[3,23,39] Such high nitrogen content should be due to the nonactivation pyrolysis process as well as the confined effect by the silica template, leading to more nitrogen atoms inserted into the carbon framework.

The surface chemical compositions of the NMCs with different nitrogen contents were analyzed by XPS, as shown in Figure 3. The survey spectra show three peaks located at 284.6, 400.0, and 513.4 eV, related to C 1s, N 1s, and O 1s,

DOI: 10.1021/acsami.5b05107
ACS Appl. Mater. Interfaces 2015, 7, 21188−21197

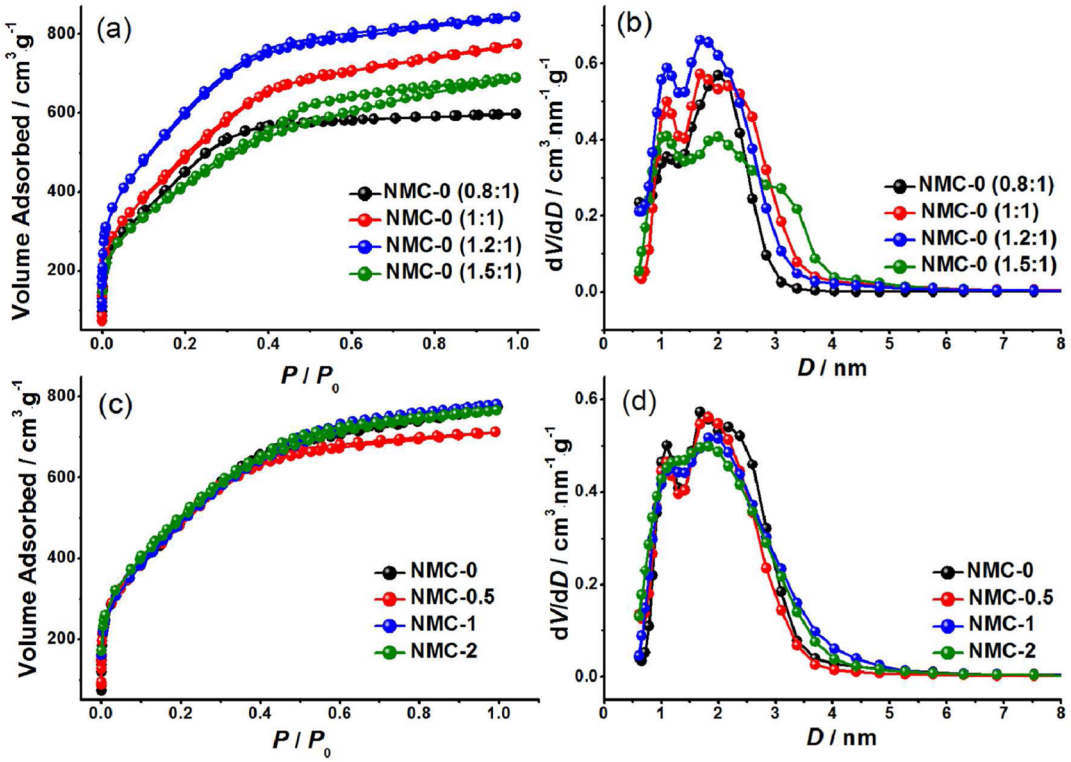

Figure 2. Nitrogen adsorption−desorption isotherms (a, c) and QS-DFT pore size distributions (b, d) of microporous carbons with different silica/phenolic resol mass ratios (a, b) and different HMMM/phenolic resol mass ratios (c, d).

Table 1. Detailed Pore Parameters of NMCs

samples	S_{BET}[a] ($m^2 \cdot g^{-1}$)	S_{DFT}[b] ($m^2 \cdot g^{-1}$)	V_t[c] ($cm^3 \cdot g^{-1}$)	V_{DFT}[d] ($cm^3 \cdot g^{-1}$)	D[e] (nm)
NMC-0	1890	900	1.2	0.6	1.9
NMC-0 (0.8:1)	1720	980	0.93	0.59	2.0
NMC-0 (1.2:1)	2260	1270	1.3	0.78	2.0
NMC-0 (1.5:1)	1530	760	1.1	0.5	2.2
NMC-0.5	1899	900	1.2	0.6	2.0
NMC-1	1885	970	1.2	0.6	2.0
NMC-2	1860	980	1.2	0.6	2.0

[a]BET specific surface area. [b]DFT micropore surface area (<2 nm). [c]Total pore volume ($P/P_0 = 0.995$). [d]DFT micropore volume (<2 nm). [e]Average pore diameter.

Table 2. Results of Elemental Analysis

samples	N (wt %)	C (wt %)	H (wt %)	O[a] (wt %)	N/C (at./at.)
NMC-0	0	91.5	1.5	7.0	0
NMC-0.5	6.3	82.9	1.9	8.9	0.065
NMC-1	8.3	79.5	2.7	9.7	0.089
NMC-2	12.1	75.6	2.0	10.3	0.14

[a]Oxygen contents were calculated based on subtraction method.

respectively (Figure 3a). The XPS spectra of C 1s (Figure 3b) show a very similar asymmetric peak shape. The main peak at 284.6 eV is related to the graphitic carbon,[40] indicating that most of the C atoms are arranged in a conjugated honeycomb lattice. The surface nitrogen contents obtained from XPS are listed in Table 3, which are significantly higher than the bulk nitrogen content from CHN analysis. This is to be expected since the nitrogen atoms are enriched at the surfaces of the pores. The XPS spectra of N 1s could be curve-fitted into four peaks with binding energies of 398.5 ± 0.3, 400.5 ± 0.3, 401.6 ± 0.3, and 404 ± 1 eV that correspond to pyridinic N (N-6), pyrrolic N (N-5), graphitic N (N-Q), and pyridine N-oxide (N-X), respectively (Figure 3c).[41,42] As shown in Figure 3d, the nitrogen-doped samples demonstrate very similar peak distributions regardless of the nitrogen content. From the peak areas, it could be concluded that most of the nitrogen species are pyridinic N and graphitic N in nature (almost 80%). Thus, the influence of nitrogen distribution can also be weakened, so only the nitrogen content should be pursued.

The microstructures of these NMCs were further revealed by XRD and Raman analysis, as shown in Figure 4. XRD patterns show very similar diffraction features with only a wide diffraction peak (2θ) at ca. 25.2, suggesting an amorphous structure with a low degree of graphitization. There are no

DOI: 10.1021/acsami.5b05107
ACS Appl. Mater. Interfaces 2015, 7, 21188−21197

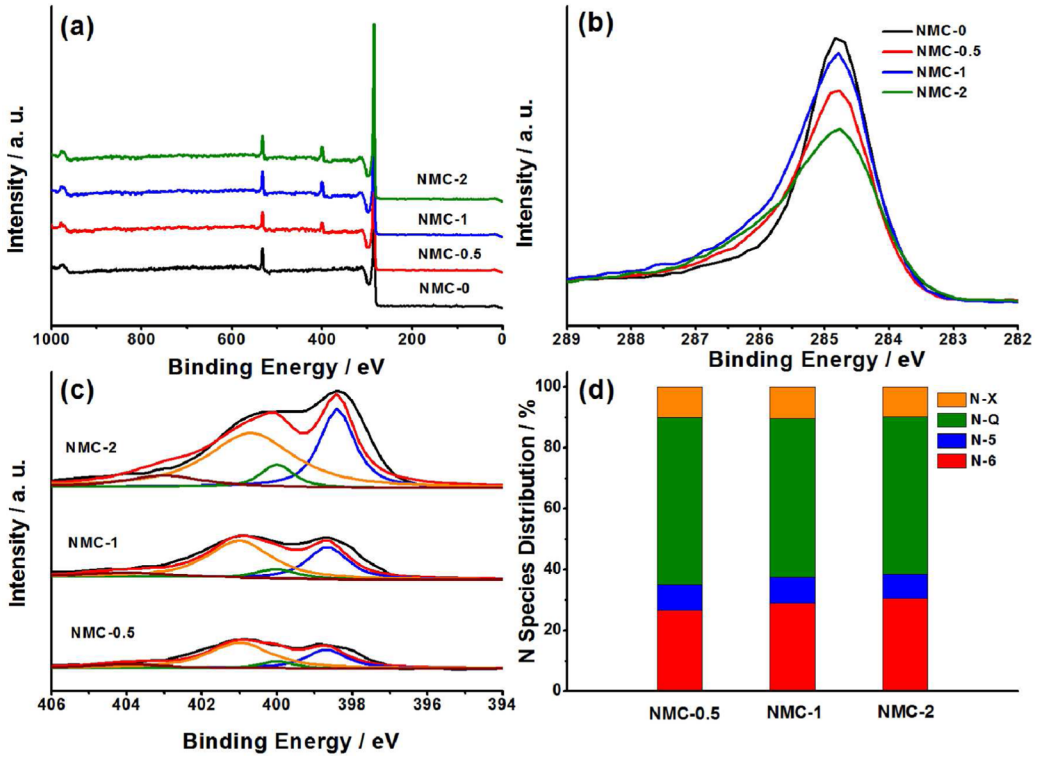

Figure 3. XPS survey (a), high-resolution C 1s (b) and N 1s (c) spectra, and the distribution of nitrogen species of the NMCs with different HMMM/phenolic resol mass ratios (d).

Table 3. Detailed Results of XPS Analysis

	elemental composition				N 1s distribution			
samples	N (at. %)	C (at. %)	O (at. %)	N/C (at./at.)	N-6[a] (%)	N-5[b] (%)	N-Q[c] (%)	N-X[d] (%)
NMC-0		84.5	15.5					
NMC-0.5	12.1	76.2	11.7	0.16	26.7	8.3	55	10
NMC-1	15.5	72.9	11.6	0.21	29	8.6	52	10.4
NMC-2	30.5	58.8	10.7	0.52	30.5	8.2	51.5	10.8

[a]Pyridinic N (398.5 ± 0.3 eV). [b]Pyrrolic N (400.5 ± 0.3 eV). [c]Graphitic N (401.6 ± 0.3 eV). [d]Pyridine N-oxide (404 ± 1 eV).

significant differences among these NMCs with different nitrogen contents. The Raman spectra of NMCs show also very similar patterns with two peaks, located at 1350 and 1580 cm^{-1}, corresponding to the D-band (disordered) and G-band (graphitic) of the carbon, respectively.[43] Generally, the relative intensities of these two lines (I_D/I_G) depend on the type of graphitic materials and are used to estimate the disordered degree of the carbon. In this work, the I_D/I_G ratios calculated from the peak area of the NMCs with the increased nitrogen contents are 1.62, 1.82, 2.13, and 2.26, respectively. This result suggests that the defectiveness of the graphite-like layers grows with increasing nitrogen content. A similar result is also found in our previous research of nitrogen-doped mesoporous carbons, indicating that the nitrogen doping could decrease the graphitization degree of the carbon.[17]

3.2. Electrochemical Performance. For the Li−S cathode, the polysulfide shuttle effect and the insulating active material are currently major technical problems. The microporous carbons have small pores for immobilizing the active material, thus limiting effectively polysulfide dissolution.[30−32] Here, in this work, the large micropore volume of as-prepared NMCs should lead to the carbon matrix holding abundant sulfur, while the high surface area is expected to restrain the polysulfide shuttle behaviors. In addition, nitrogen doping can be directly utilized to absorb soluble Li_2S_x, showing unprecedentedly strong adsorption abilities and can thus efficiently trap lithium polysulfides within the cathodes.[44−48] More importantly, the as-prepared NMCs are largely structurally similar with respect to the same template, and the major variable is the nitrogen content doped. It is, therefore, possible to probe how changes in nitrogen doping content affect the performance of the carbons. Here, this work takes sulfur/carbon composite cathodes for a Li−S battery as examples, but the concept should be applicable to many other systems such as supercapacitors and CO_2 adsorption as well.

The binary NMC/S composite cathodes were prepared via a conventional melt impregnation process. The sulfur content of these composites is carefully controlled to be the same with 40 wt % sulfur, as confirmed by TGA results (Figure 5a). In addition, it can be seen that the weight loss onset temperature, responding to sulfur evaporation, generally increases with the nitrogen content. The reason for this might be associated with the strong surface interaction of the basic nitrogen species and sulfur, suggesting a good immobilization capability of the nitrogen-doped carbon matrix. After sulfur impregnation, no

DOI: 10.1021/acsami.5b05107
ACS Appl. Mater. Interfaces 2015, 7, 21188−21197

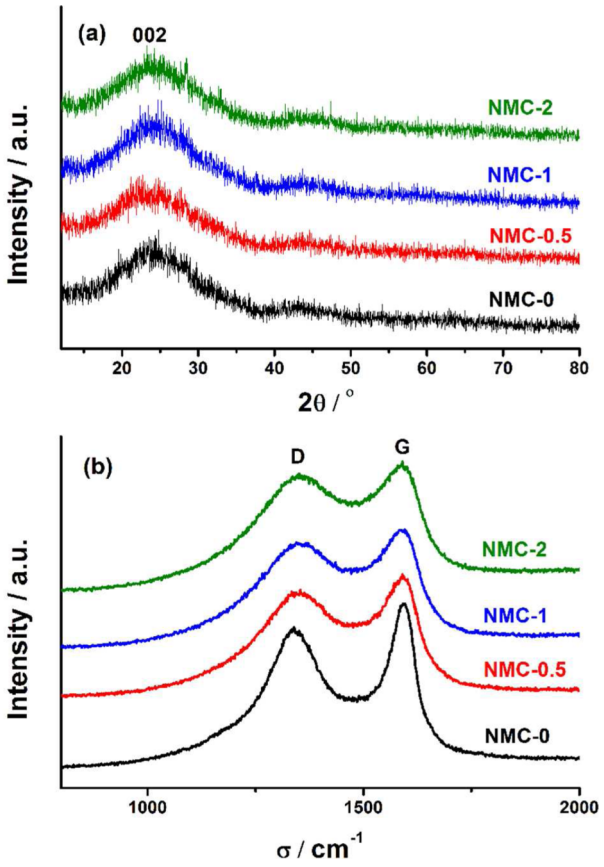

Figure 4. XRD patterns (a) and Raman spectra (b) of NMCs with different nitrogen contents.

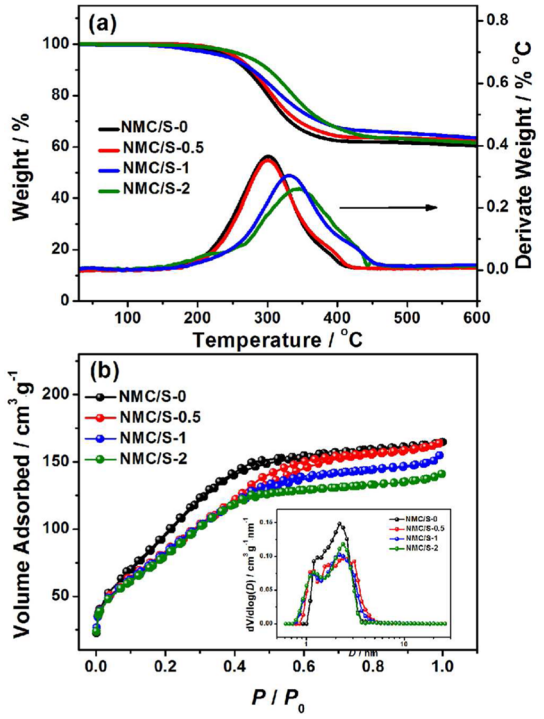

Figure 5. Thermogravimetric (a) and nitrogen adsorption−desorption analysis (b) of NMC/S composites with different nitrogen contents.

sulfur peaks can be observed in XRD (Figure S6, Supporting Information), suggesting that sulfur is homogeneously distributed into the pores of NMCs without being aggregated. The binary NMC/S composites still possess considerable microporous structures, as revealed by N_2 adsorption in Figure 5b. Detailed porosity properties are summarized in Table S1. All the samples exhibit similar porosity with surface areas of 350−400 $m^2 \cdot g^{-1}$ and pore volumes of 0.22−0.26 $cm^3 \cdot g^{-1}$. Such considerable surface areas and pore volumes of the NMC/S composites are favorable for the access connection of the electrolyte throughout the microporous structure of the NMCs. In addition, the residual porosity should also accommodate the large volumetric expansion of sulfur during cycling.

The electrochemical behaviors of these NMC/S composites are evaluated by using cycle voltammetry (CV), galvanostatic charge−discharge testing, and electrochemical impedance spectroscopy (EIS). The CV curves of the NMC/S composites at a scanning rate of 0.2 $mV \cdot S^{-1}$ during the second cycle are shown in Figure 6. Two well-defined reduction peaks are

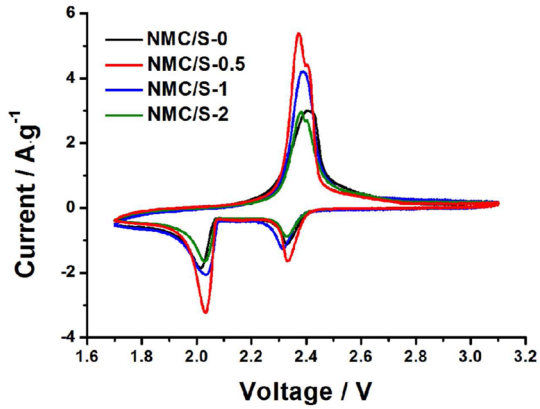

Figure 6. Typical CV curves of NMC/S composites at a scan rate of 0.2 $mV \cdot S^{-1}$ in a voltage range of 1.6−3.1 V.

observed for all composites, in which the first peak in the range of 2.30−2.35 V relates to the reduction of S_8 to high-order lithium polysulfide (Li_2S_x, $4 \le x \le 8$), while the second peak in the range of 2.01−2.09 V relates to the strong reduction of soluble polysulfide anions to an insoluble Li_2S_2/Li_2S deposit. In the subsequent anodic scan, only one asymmetric oxidation peak is observed at ca. 2.39 V, attributed to the conversion of lithium sulfides to polysulfides and sulfur.[49] Except for the intensity difference of these peaks, no other obvious differences including the sulfur reduction onset potential are observed for these composites with different nitrogen contents. This suggests that the nitrogen doping level does not affect the redox-reduction reaction process.

The charge and discharge voltage profiles of NMC/S composites at a current density of 837.5 $mA \cdot g^{-1}$ (0.5 C) are presented in Figure 7a. During the discharge process, there are two plateaus (around 2.3 and 2.1 V, respectively) like all the sulfur-containing cathodes, corresponding to the formation of long-chain polysulfides (Li_2S_x, $4 \le x \le 8$) at the high plateau and short-chain polysulfides (Li_2S_x, $1 \le x \le 2$) at the low plateau.[26] In Figure 7b, the initial capacities of these composites are greatly different, with an order of NMC/S-0.5, NMC/S-1, NMC/S-0, and NMC/S-2. The initial capacity difference should be directly related to the nitrogen content, which is the major difference between these NMC/S composites.[44−46] Among the samples investigated, the NMC/S-0.5 with the mediate nitrogen content (6.3 wt %) exhibits the highest initial

DOI: 10.1021/acsami.5b05107
ACS Appl. Mater. Interfaces 2015, 7, 21188−21197

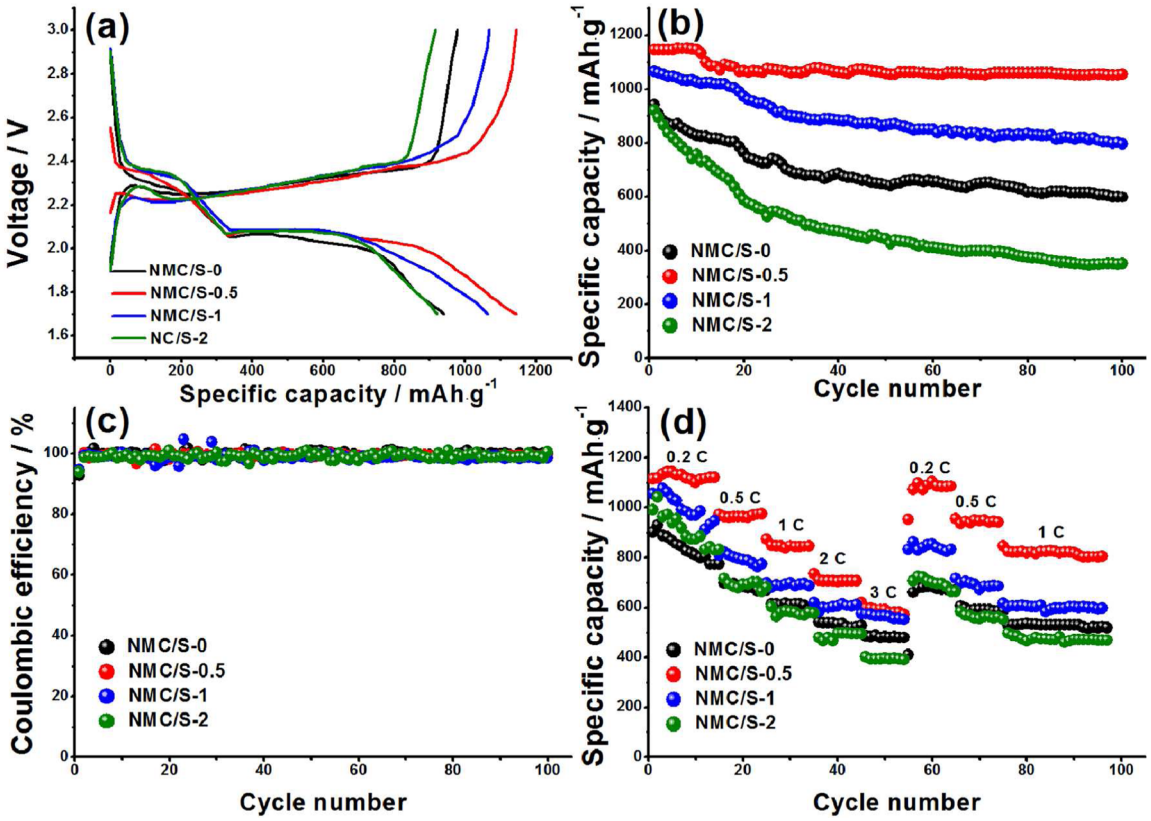

Figure 7. Charge−discharge profiles at 0.5 C (a), cyclic performance at 0.5 C (b), Coulombic efficiency (c), and rate performance (d) of NMC/S composites with different nitrogen contents.

capacity of 1150 mAh·g^{-1}. After 100 cycles, the NMC/S-0.5 exhibits the best cyclic stability; about 95% of the capacity (1054 mAh·g^{-1}) is maintained with a decay of only 0.1% per cycle. The Coulombic efficiencies of all samples are shown in Figure 7c. All of these samples possess very high Coulombic efficiencies of ca. 92−94% in the first cycle. During the following cycles, the Coulombic efficiency was as high as 98−100%, which may be ascribed to the following two reasons. On the one hand, $LiNO_3$ added into the electrolyte could continuously react with lithium metal to generate a protective film on the surface of lithium, preventing the polysulfides from contacting with lithium metal directly.[50,51] On the other hand, the small pores have strong immobilizing ability for the active material, thus limiting effectively polysulfide dissolution.[32] The rate capabilities of these composites are compared in Figure 7d. After 15 cycles at 0.2 C, the NMC/S-0.5 exhibits the highest reversible capacity of 1150 mAh·g^{-1}. At the maximum discharge rate of 3 C, it still delivers a high capacity of 550 mAh·g^{-1}, much higher than other samples. Regardless of the sulfur loading, such cyclic ability and rate performance are among the highest in the reported results of sulfur/carbon composites.[27−31,52]

The nitrogen functionalities are often directly doped into the carbon framework, which could provide hydrophilic ability and Lewis basic properties, serving as immobilizers to anchor polysulfide anions and retarding their diffusion. However, it should be noted that the electrochemical performances strongly depended on the nitrogen content of microporous carbons. When the nitrogen content is increased to 12 wt %, the capacity of the NMC/S-2 composites decreases to 350 mAh·g^{-1} after 100 cycles at 0.5 C, much lower than that of the NMC/S-0.5 and the NMC/S-1 composites with mediate nitrogen contents. This should be owing to the significant deterioration of electronic conductivity caused by the excessive nitrogen doping. To confirm it, the powder electrical conductivities of these NMCs with different nitrogen contents were measured using a four-probe method. As shown in Figure 8a, compared to nitrogen-free NMC-0, only a mediate nitrogen content (6−8 wt %) can greatly increase the electronic conductivity; otherwise, excessive nitrogen content results in a remarkable deterioration of the conductivity. This should be due to the trade-off between two independent effects issued from nitrogen doping. On one hand, doping higher electronegativity nitrogen into the carbon framework can improve the electronic conductivity of the carbon. On the other hand, excessive nitrogen doping interrupts the interconnections of the graphitic structure, leading to the decrease of conductivity. After sulfur loading, the electron conductivity changes slightly. This result indicates that the sulfur is homogeneously distributed into the pores of NMCs and the electric conductivity network has not been interrupted.[44] The EIS results (Figure 8b) are in good agreement with the results of electronic conductivity. The semicircle diameter in the high frequency region of Nyquist plots indicates that the charge-transfer kinetics are the fastest in NMC/S-0.5 composites. Thus, it can be concluded that only mediate nitrogen doping leads to a substantial increase in the electrochemical performance of the NMC/S composites. Excessive nitrogen doping even causes a detrimental effect on the materials.

DOI: 10.1021/acsami.5b05107
ACS Appl. Mater. Interfaces 2015, 7, 21188−21197

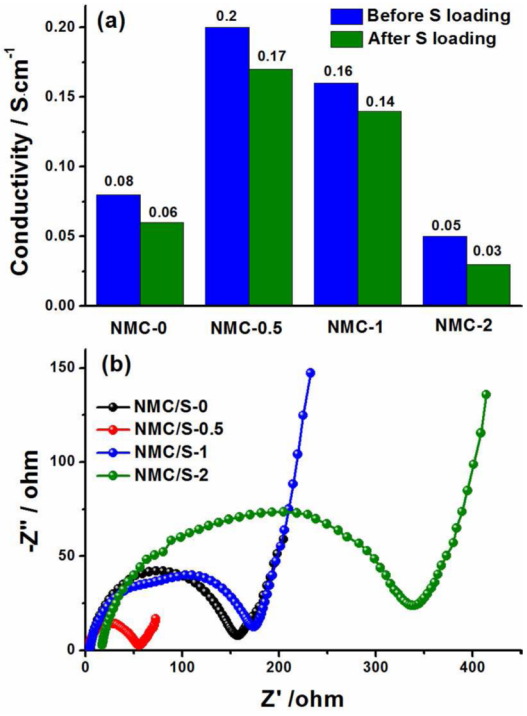

Figure 8. Electronic conductivity (a) and EIS (b) of NMCs with different nitrogen contents.

4. CONCLUSIONS

Nitrogen-doped microporous carbons with highly developed microporous structures and controllable nitrogen contents were successfully prepared via a simple and versatile organic–inorganic sol–gel process. The uniform micropores are created by replicating the low-degree-hydrolysis silica template, while controllable nitrogen doping could be achieved by changing the precursor composition. This synthesis method is very flexible, allowing easy control of the microporous structure and nitrogen content. The obtained NMCs have very large BET surface areas of 1530–2260 $m^2 \cdot g^{-1}$, high pore volumes of 0.9–1.3 $cm^3 \cdot g^{-1}$, and narrow pore size distributions of 1–3 nm. In addition, the nitrogen content doped into the carbon framework can be easily adjusted in a wide range from 0 to 12.1 wt %, while the microporous structure can be kept almost the same. This, therefore, allowed these materials to serve as model systems for microporous carbons in general, to illustrate the role of nitrogen doping on the performance of microporous carbons. When used as supports for sulfur/carbon cathodes, it shows a clear nitrogen content dependent electrochemical performance. Only an appropriate level of nitrogen doping (6.3%) is effective to greatly improve sulfur utilization and cycle life of the sulfur/carbon composites. These results should be of great interest in understanding the nitrogen doping promoted performance of microporous carbons, which should provide a useful guide for controlling the nitrogen-doped surface chemistry for many related applications.

■ ASSOCIATED CONTENT

Supporting Information

The Supporting Information is available free of charge on the ACS Publications website at DOI: 10.1021/acsami.5b05107.

Figures showing the GPC results of phenolic resol, the digital photograph of alcogel, the TEM images of NMCs with different nitrogen contents, the TG results of C/silica composites and resulting NMCs, and the XRD patterns of NMC/S composites (PDF)

■ AUTHOR INFORMATION

Corresponding Author

*Tel: +86 21 64252924. Fax: +86 21 64252914. E-mail: longdh@mail.ecust.edu.cn.

Author Contributions

The manuscript was written through contributions of all authors. All authors have given approval to the final version of the manuscript.

Notes

The authors declare no competing financial interest.

■ ACKNOWLEDGMENTS

This work was partly supported by MOST (2014CB239702) and the National Science Foundation of China (Nos. 51302083, 51172071, 51272077), and Fundamental Research Funds for the Central Universities and Shanghai Rising Star Program (15QA1401300).

■ REFERENCES

(1) Lee, J.; Kim, J.; Hyeon, T. Recent Process in the Synthesis of Porous Carbon Materials. *Adv. Mater.* **2006**, *18*, 2073–2094.
(2) Rzepka, M.; Lamp, P.; de la Casa-Lillo, M. A. Physisorption of Hydrogen on Microporous Carbon and Carbon Nanotubes. *J. Phys. Chem. B* **1998**, *102*, 10894–10898.
(3) Su, F.; Poh, C.; Chen, J.; Xu, G.; Wang, D.; Li, Q.; Lin, J.; Lou, X. Nitrogen-Containing Microporous Carbon Nanospheres with Improved Capacitive Properties. *Energy Environ. Sci.* **2011**, *4*, 717–724.
(4) Ma, Z.; Kyotani, T.; Liu, Z.; Terasaki, O.; Tomita, A. Very High Surface Area Microporous Carbon with a Three-Dimensional Nano-Array Structure: Synthesis and Its Molecular Structure. *Chem. Mater.* **2001**, *13*, 4413–4415.
(5) Hu, Z.; Srinivasan, M.; Ni, Y. Novel Activation Process for Preparing Highly Microporous and Mesoporous Activated Carbons. *Carbon* **2001**, *39*, 877–886.
(6) Saleh, M.; Chandra, V.; Kemp, K. C.; Kim, K. S. Synthesis of N-doped Microporous Carbon via Chemical Activation of Polyindole-Modified Graphene Oxide Sheets for Carbon Dioxide Adsorption. *Nanotechnology* **2013**, *24*, 255702.
(7) Sircar, S.; Golden, T.; Rao, M. Activated Carbon for Gas Separation and Storage. *Carbon* **1996**, *34*, 1–12.
(8) Meisner, G. P.; Hu, Q. High Surface Area Microporous Carbon Materials for Cryogenic Hydrogen Storage Synthesized Using New Template-based and Activation-Based Approaches. *Nanotechnology* **2009**, *20*, 204023.
(9) Matranga, K.; Myers, A.; Glandt, E. Storage of Natural Gas by Adsorption on Activated Carbon. *Chem. Eng. Sci.* **1992**, *47*, 1569–1579.
(10) Kyotani, T.; Nagai, T.; Inoue, S.; Tomita, A. Formation of New Type of Porous Carbon by Carbonization in Zeolite Nanochannels. *Chem. Mater.* **1997**, *9*, 609–615.
(11) Ma, Z.; Kyotani, T.; Tomita, A. Preparation of a High Surface Area Microporous Carbon Having the Structure Regularity of Y Zeolite. *Chem. Commun.* **2000**, *23*, 2365–2366.
(12) Matsuoka, K.; Yamagishi, Y.; Yamazaki, T.; Setoyama, N.; Tomita, A.; Kyotani, T. Extremely High Microporosity and Sharp Pore Size Distribution of a Large Surface Area Carbon Prepared in the Nanochannels of Zeolite Y. *Carbon* **2005**, *43*, 876–879.
(13) Li, Z.; Wu, D.; Liang, Y.; Fu, R.; Matyjaszewski, K. Synthesis of Well-Defined Microporous Carbons by Molecular-Scale Templating with Polyhedral Oligomeric Silsesquioxane Moieties. *J. Am. Chem. Soc.* **2014**, *136*, 4805–4808.

DOI: 10.1021/acsami.5b05107
ACS Appl. Mater. Interfaces 2015, 7, 21188–21197

(14) Seredych, M.; Hulicova-Jurcakova, D.; Lu, G.; Bandosz, T. Surface Functional Groups of Carbons and the Effects of Their Chemical Character, Density and Accessibility to Ions on Electrochemical Performance. *Carbon* **2008**, *46*, 1475−1488.
(15) Zhao, X.; Zhao, H.; Zhang, T.; Yan, X.; Yuan, Y.; Zhang, H.; Zhao, H.; Zhang, D.; Zhu, G.; Yao, X. One-Step Synthesis of N-Doped Microporous Carbon Materials as Metal-Free Electrocatalysts for Oxygen Reduction Reaction. *J. Mater. Chem. A* **2014**, *2*, 11666−11671.
(16) Chen, L.; Zhang, X.; Liang, H.; Kong, M.; Guan, Q.; Chen, P.; Wu, Z.; Yu, S. Synthesis of Nitrogen-Doped Porous Carbon Nanofibers as an Efficient Electrode Material for Supercapacitors. *ACS Nano* **2012**, *6*, 7092−7102.
(17) Chen, H.; Sun, F.; Wang, J.; Li, W.; Qiao, W.; Ling, L.; Long, D. Nitrogen Doping Effects on the Physical and Chemical Properties of Mesoporous Carbons. *J. Phys. Chem. C* **2013**, *117*, 8318−8328.
(18) Shao, Y.; Sui, J.; Yin, G.; Gao, Y. Nitrogen-Doped Carbon Nanostructures and Their Composites As Catalytic Materials for Proton Exchange Membrane Fuel Cells. *Appl. Catal., B* **2008**, *79*, 89−99.
(19) Hao, G.; Li, W.; Qian, D.; Lu, A. Rapid Synthesis of Nitrogen-Doped Porous Carbon Monolith for CO_2 Capture. *Adv. Mater.* **2010**, *22*, 853−857.
(20) Qie, L.; Chen, W.-M.; Wang, Z.-H.; Shao, Q.-G.; Li, X.; Yuan, L.-X.; Hu, X.-L.; Zhang, W.-X.; Huang, Y.-H. Nitrogen-doped Porous Carbon Nanofiber Webs as Anodes for Lithium Ion Batteries with a Super High Capacity and Rate Capability. *Adv. Mater.* **2012**, *24*, 2047−2050.
(21) Kim, K.; Park, S. Synthesis and High Electrochemical Capacitance of N-Doped Microporous Carbon/Carbon Nanotubes for Supercapacitor. *J. Electroanal. Chem.* **2012**, *673*, 58−64.
(22) Ania, C.; Khomenko, V.; Raymundo-Piñero, E.; Parra, J.; Beguin, F. The Large Electrochemical Capacitance of Microporous Doped Carbon Obtained by Using a Zeolite Template. *Adv. Funct. Mater.* **2007**, *17*, 1828−1836.
(23) Hou, P.; Orikasa, H.; Yamazaki, T.; Matsuoka, K.; Tomita, A.; Setoyama, N.; Fukushima, Y.; Kyotani, T. Synthesis of Nitrogen-containing Microporous Carbon with a Highly Ordered Structure and Effect of Nitrogen Doping on H_2O Adsorption. *Chem. Mater.* **2005**, *17*, 5187−5193.
(24) Xia, Y.; Walker, G.; Grant, D.; Mokaya, R. Hydrogen Storage in High Surface Area Carbons: Experimental Demonstration of the Effects of Nitrogen Doping. *J. Am. Chem. Soc.* **2009**, *131*, 16493−16499.
(25) Xia, Y.; Mokaya, R.; Walker, G.; Zhu, Y. Superior CO_2 Adsorption Capacity on N-Doped, High-Surface-Area, Microporous Carbons Templated from Zeolite. *Adv. Energy Mater.* **2011**, *1*, 678−683.
(26) Lin, Z.; Liang, C. Lithium-Sulfur Batteries: From Liquid to Solid Cell. *J. Mater. Chem. A* **2015**, *3*, 936−958.
(27) Wang, Z.; Dong, Y.; Li, H.; Zhao, Z.; Wu, H. B.; Hao, C.; Liu, S.; Qiu, J.; Lou, X. W. Enhancing Lithium−Sulphur Battery Performance by Strongly Binding the Discharge Products on Amino-Functionalized Reduced Graphene Oxide. *Nat. Commun.* **2014**, *5*, 5002.
(28) Xin, S.; Yin, Y.; Wan, L.; Guo, Y. Encapsulation of Sulfur in a Hollow Porous Carbon Substrate for Superior Li − S Batteries with Long Lifespan. *Par. Par. Syst. Char.* **2013**, *30*, 321−325.
(29) Liang, X.; Wen, Z.; Liu, Y.; Zhang, H.; Huang, L.; Jin, J. Highly Dispersed Sulfur in Ordered Mesoporous Carbon Sphere as a Composite Cathode for Rechargeable Polymer Li/S Battery. *J. Power Sources* **2011**, *196*, 3655−3658.
(30) Su, Y.-S.; Manthiram, A. Lithium-Sulfur Batteries with a Microporous Carbon Paper as a Bifunctional Interlayer. *Nat. Commun.* **2012**, *3*, 1166.
(31) Elazari, R.; Salitra, G.; Garsuch, A.; Panchenko, A.; Aurbach, D. Sulfur Impregnated Activated Carbon Fiber Cloth as a Binder-Free Cathode for Rechargeable Li-S Batteries. *Adv. Mater.* **2011**, *23*, 5641−5644.
(32) Zhang, L.; Qin, X.; Li, G.; Gao, X. Enhancement of Long Stability of Sulfur Cathode by Encapsulating Sulfur into Micropores of Carbon Spheres. *Energy Environ. Sci.* **2010**, *3*, 1531−1537.
(33) Manthiram, A.; Fu, Y.; Chung, S.; Zu, C.; Su, Y. Rechargeable Li-Sulfur Batteries. *Chem. Rev.* **2014**, *114*, 11751−11787.
(34) Zhao, C.; Liu, L.; Zhao, H.; Krall, A.; Wen, Z.; Chen, J.; Hurley, P.; Jiang, J.; Li, Y. Sulfur-Infiltrated Porous Carbon Microspheres with Controllable Multi-Modal Pore Size Distribution for High Energy Lithium−Sulfur Batteries. *Nanoscale* **2014**, *6*, 882−888.
(35) Wang, D.; Zeng, Q.; Zhou, G.; Yin, L.; Li, F.; Cheng, H.; Gentle, I.; Lu, G. Carbon-Sulfur Composites for Li-S Batteries: Status and Prospects. *J. Mater. Chem. A* **2013**, *1*, 9382−9394.
(36) Kailasam, K.; Jun, Y.; Katekomol, P.; Epping, J.; Hong, W.; Thomas, A. Mesoporous Melamine Resins by Soft Templating of Block-Co-Polymer Mesophases. *Chem. Mater.* **2010**, *22*, 428−434.
(37) Meng, Y.; Gu, D.; Zhang, F.; Shi, Y.; Yang, H.; Li, Z.; Yu, C.; Tu, B.; Zhao, D. Ordered Mesoporous Polymers and Homologous Carbon Frameworks: Amphiphilic Surfactant Templating and Direct Transformation. *Angew. Chem.* **2005**, *117*, 7215−7221.
(38) He, G.; Ji, X.; Nazar, L. High "C" Rate Li-S Cathodes: Sulfur Imbibed Bimodal Porous Carbons. *Energy Environ. Sci.* **2011**, *4*, 2878−2883.
(39) Wang, J.; Senkovska, I.; Oschatz, M.; Lohe, M.; Borchardt, L.; Heerwig, A.; Liu, Q.; Kaskel, S. Imine-Linked Polymer-Derived Nitrogen-Doped Microporous Carbons with Excellent CO_2 Capture Properties. *ACS Appl. Mater. Interfaces* **2013**, *5*, 3160−3167.
(40) Lee, W.; Lee, J.; Reucroft, P. XPS Study of Carbon Fiber Surface Treated by Thermal Oxidation in a Gas Mixture of $O_2/(O_2+N_2)$. *Appl. Surf. Sci.* **2001**, *171*, 136−142.
(41) Morant, C.; Andrey, J.; Prieto, P.; Mendiola, D.; Sanz, J. M.; Elizalde, E. XPS Characterization of Nitrogen-Doped Carbon Nanotubes. *Phys. Status Solidi A* **2006**, *203*, 1069−1075.
(42) Park, K.; Jang, J.; Hong, J.; Kwon, Y. Mesoporous Thin Films of Nitrogen-Doped Carbon with Electrocatalytic Properties. *J. Phys. Chem. C* **2012**, *116*, 16848−16853.
(43) Mcguire, K.; Gothard, N.; Gai, P.; Dresselhaus, M.; Sumanasekera, G.; Rao, A. Synthesis and Raman Characterization of Single-walled Carbon Nanotubes. *Carbon* **2005**, *43*, 219−227.
(44) Sun, X. G.; Wang, X. Q.; Mayes, R. T.; Dai, S. Li-S Batteries Based on Nitrogen-Doped Porous Carbon and an Ionic-liquid Electrolyte. *ChemSusChem* **2012**, *5*, 2079−2085.
(45) Sun, F.; Wang, J. T.; Chen, H.; Li, W.; Qiao, W.; Long, D.; Ling, L. High Efficiency Immobilization of Sulfur on Nitrogen-Enriched Mesoporous Carbons for Li-S Batteries. *ACS Appl. Mater. Interfaces* **2013**, *5*, 5630−5638.
(46) Wang, X.; Zhang, Z.; Qu, Y.; Lai, Y.; Li, J. Nitrogen-Doped Graphene/Sulfur Composite as Cathode Material for High Capacity Lithium−Sulfur Batteries. *J. Power Sources* **2014**, *256*, 361−368.
(47) Yang, J.; Xie, J.; Zhou, X.; Zou, Y.; Tang, J.; Wang, S.; Chen, F.; Wang, L. Functionalized N-doped Porous Carbon Nanofiber Webs for a Li-Sulfur Battery with High Capacity and Rate Performance. *J. Phys. Chem. C* **2014**, *118*, 1800−1807.
(48) Song, J.; Gordin, M.; Xu, T.; Chen, S.; Yu, Z.; Sohn, H.; Lu, J.; Ren, Y.; Duan, Y.; Wang, D. Strong Lithium Polysulfide Chemisorption on Electroactive Sites of Nitrogen-Doped Carbon Composites For High-Performance Lithium−Sulfur Battery Cathodes. *Angew. Chem., Int. Ed.* **2015**, *54*, 4325−4329.
(49) Jayaprakash, N.; Shen, J.; Moganty, S.; Corona, A.; Archer, L. Porous Hollow Carbon@Sulfur Composites for High-Power Lithium-Sulfur Batteries. *Angew. Chem.* **2011**, *123*, 6026−6030.
(50) Zheng, G.; Yang, Y.; Cha, J.; Hong, S. S.; Cui, Y. Hollow Carbon Nanofiber-Encapsulated Sulfur Cathodes for High Specific Capacity Rechargeable Lithium Batteries. *Nano Lett.* **2011**, *11*, 4462−4467.
(51) Liang, X.; Wen, Z.; Liu, Y.; Wu, M.; Jin, J.; Zhang, H.; Wu, X. Improved Cycling Performances of Lithium Sulfur Batteries with $LiNO_3$-Modified Electrolyte. *J. Power Sources* **2011**, *196*, 9839−9843.
(52) Zhang, W.; Qiao, D.; Pan, J.; Cao, Y.; Yang, H.; Ai, X. A Li^+ Conductive Microporous Carbon-Sulfur Composites for Li-S Batteries. *Electrochim. Acta* **2013**, *87*, 497−502.

DOI: 10.1021/acsami.5b05107
ACS Appl. Mater. Interfaces 2015, 7, 21188−21197